Electrochemical and Solid-State Letters, **11** (8) B127-B131 (2008)
1099-0062/2008/11(8)/B127/5/$23.00 © The Electrochemical Society

Measurement of Capillary Pressure Property of Gas Diffusion Media Used in Proton Exchange Membrane Fuel Cells

T. V. Nguyen,[z] G. Lin, H. Ohn, and X. Wang*

Chemical and Petroleum Engineering Department, The University of Kansas, Lawrence, Kansas 66045, USA

This work presents an experimental method that is one of the few to allow both imbibition and drainage capillary measurement at pressures above breakthrough. It was used on Toray and SGL Carbon gas diffusion materials at room temperature. These materials exhibited both hydrophobic and hydrophilic properties. Breakthrough pressures for Toray and SGL Carbon were 3.6 and 1.5 kPa, respectively. Little hysteresis was observed in these room-temperature experiments, which is an interesting contrast with the results from the only other group, Schwartz's group at University of Washington, to measure these properties. A double exponential equation was used to fit the data for each carbon paper.
 [DOI: 10.1149/1.2929063]

Manuscript submitted August 29, 2007; revised manuscript received April 21, 2008. Available electronically May 23, 2008.

In a hydrogen proton exchange membrane fuel cell (PEMFC), liquid water is generated as a by-product $[O_{2(g)} + 4H^+ + 4e^- \leftrightarrow 2H_2O_{(l)}]$ at the cathode during operation. When the generation rate of liquid water exceeds its removal rate, liquid water accumulates in the gas diffusion and catalyst layers of the cathode and affects the transport rates of the reactants and products to and from the reactive sites in the electrodes by (*i*) reducing the effective cross-sectional area for gas transport and (*ii*) acting as an additional diffusion barrier by forming a thin film over the catalyst surface. Furthermore, by reducing the gas volume in the porous components of the cathode that could be immediately available for reaction, liquid water accumulation affects the transient performance of the PEMFC. In a direct methanol fuel cell (DMFC), in addition to the two-phase condition in the cathode similar to that in a hydrogen PEMFC, another two-phase condition also exists in the anode when gaseous carbon dioxide is generated as a by-product of the (liquid) methanol reaction $[CH_3OH_{(l)} + H_2O_{(l)} \leftrightarrow CO_{2(g)} + 6H^+ + 6e^-]$ during operation. The transport rates of gas and liquid in the porous layers in a fuel cell depend greatly on two main two-phase transport properties of these components: the capillary pressure and the relative permeability of gas and liquid. These two-phase transport properties, which depend on the morphological and wetting properties of the materials used, are often correlated to the liquid water saturation level in the components.

It is obvious from the discussion above that two-phase transport properties of materials used in PEMFCs are needed to optimize fuel cell electrodes (catalyst and gas diffusion layers) to have better fuel cell performance. Furthermore, for fuel cell models[1-14] to provide accurate evaluations of flow field designs and operating conditions needed for optimal fuel cell performance, accurate two-phase flow properties are required. Given the importance of two-phase transport properties of the gas diffusion materials used in PEMFCs in the analysis of the effects of liquid water flooding on the performance of these fuel cells, it is surprising that only a very limited number of studies on two-phase transport properties of the actual materials used in PEMFCs have been published.[15-26] Because of the lack of data, many two-phase flow models recently developed for PEMFCs and DMFCs had resorted to using capillary pressure data correlated for porous geological materials (e.g., sand), mainly the empirical correlation developed by Udell.[27] The use of Udell's correlation in these models[2,5,8,11,13,14] has often led to predicted liquid water saturation levels in the gas diffusion components that were unrealistically low. Recent diagnostic tools, such as pressure drop measurement with interdigitated flow field and neutron radiography, have confirmed that the liquid water saturation levels in the gas diffusion components were many times higher than those predicted by these models. To help fill this information gap, efforts in this area have started at a few locations and the results are beginning to appear in the literature.[16-26] This paper discusses a technique that we have developed for measuring the capillary pressure properties of porous carbon materials used as the gas diffusion layers (GDLs) in PEMFCs and the results obtained for some commercially available materials.

Experimental

Apparatus.— The technique adopted for the capillary pressure measurement of gas diffusion materials used in PEMFCs in this study was based on a volume-displacement technique developed by Morrow and Mungan[28] and Morrow.[29] This technique can be used to measure the capillary pressure properties of both hydrophilic and hydrophobic porous materials. The main requirement is that the sample must have sufficient pore volume to allow accurate measurement of the displaced volume. The procedure involves filling and draining water into and from the sample by varying the liquid water pressure at the water and sample interface and measuring the volume of the displaced water. Because there were many issues that we had to resolve before reproducible measurements could be made, we tried to provide as much detail as possible so that others can repeat these measurements.

Figure 1 shows a schematic of the capillary measurement setup, which includes three main components, the sample holder, the connecting tubing, and the volume-displacement measurement horizontal tube. Note that the two outlets open to the atmosphere were exposed to water-saturated air at atmospheric pressure to minimize water loss by evaporation. Also, the apparatus was placed in a supported temperature-controlled chamber to shield it from large temperature variations in the lab and vibrations in the building during the measurements.

The sample holder includes two end plates, a top made of plastic and a bottom made of stainless steel, with compartments in which

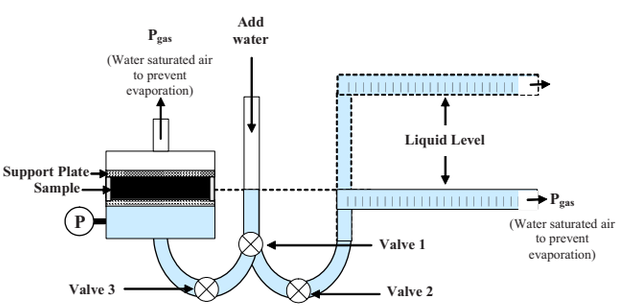

Figure 1. (Color online) Schematic of the volume displacement experimental setup.

* Electrochemical Society Student Member.
[z] E-mail: cptvn@ku.edu

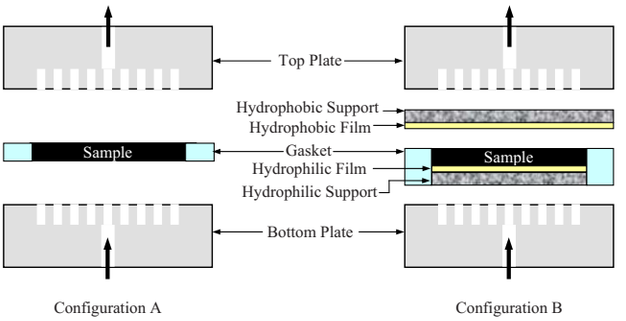

Figure 2. (Color online) Configurations used in the capillary pressure measurements: (A) For natural breakthrough points and (B) beyond natural breakthrough points.

crosswise channels were machined to create islands that provided support for the sample at the top and bottom. Water was introduced into the chamber through an opening in the bottom. Stainless steel material was used for its corrosion resistance and high surface wetting property. Note that metal ions generated by corrosion could affect the wetting property of the sample. Strong wettability is necessary to allow water to fill the compartment in the bottom plate without entrapped air pockets.

The machined compartments in both the top and bottom plates were $60 \times 60 \times 5$ mm (depth), and the sample was 66×66 mm by the thickness of the sample. For a sample of 300 μm in thickness and 85% in porosity, these dimensions allow 0.918 mL of water to be imbibed at full saturation. A layer of gasket made of expanded Teflon sealed the edges of the sample. Two configurations were used. Configuration A, which was used to obtain the capillary pressure curve up to the sample bubble point and the point where liquid water breaks through the sample, consisted of only the sample between two end plates. Configuration B, which was used to measure the capillary pressure beyond the liquid breakthrough point and the bubble point of the sample, consisted of two additional hydrophilic porous layers below the sample and two hydrophobic porous layers above the sample. The hydrophobic layer in contact with the top surface of the sample was a GE hydrophobic nylon membrane (model no. R99SH320F5) with 10 μm average pore size and 17.2 kPa water breakthrough pressure. Note that the water breakthrough point of these GDL samples varied between 1.5 and 4 kPa. A 10% wet proof porous carbon paper (from SGL Carbon) was used as the support for the soft hydrophobic nylon film. The bottom hydrophilic layer in contact with the bottom surface of the sample was a GE hydrophilic nylon membrane (model no. R12SP14225) with 1.2 μm average pore size and 77 kPa bubble pressure. A 0% wet proof porous carbon paper (from SGL Carbon) made hydrophilic by soaking in Nafion solution and heat-treated at 130°C for 20 min was used as the support for the bottom hydrophilic nylon film.

Figure 2 shows the arrangement of the components in configurations A and B. Note that the liquid water breakthrough point obtained in configuration A is of great interest because in a PEMFC one face of the GDL is exposed to the gas channels. The capillary pressure encountered in a working fuel cell would not exceed the liquid water breakthrough point. However, for the purpose of material characterization and generating capillary pressure correlation that covers a capillary pressure range beyond the liquid water breakthrough point, configuration B was used.

The connecting tubing between the horizontal tubing and the sample holder should be rigid to prevent swelling or contraction when the liquid pressure changes, which could lead to inaccurate measurements of the displaced volume. For the displaced volume measurement tube, a 1.9 mm i.d. (± 0.05 mm), 120 cm long Teflon tube was used to allow an accurate reading of the small volume change involved in these measurements. Teflon was used to prevent creation of another capillary interface at the air and water interface at the end that was exposed to air. Finally, the big vertical tube along with three valves was used to allow water to be added to either the chamber or the horizontal displacement measurement tube.

Procedure.— Capillary pressure measurement typically involves first saturating the sample with a liquid and then cycling between draining and imbibing the liquid from and into the sample by either raising the gas pressure or reducing the liquid pressure and vice versa. The first step is called the fill-up step, which involves the movement of water into a totally dry sample. The second curve is the first drainage curve of the capillary pressure curve followed by the first imbibition curve. These drainage and imbibition capillary pressure curves represent the interaction between three phases (solid, liquid, and gas) as the saturation level decreases and increases. It has been reported by Anderson[30] that spontaneous imbibition of water can occur with porous materials having water surface contact angles of $<50^{\circ}$. For materials with water contact angles of $>50^{\circ}$, forced imbibition is required. That is, the liquid pressure has to be higher than the gas pressure to force water into the sample. Once the sample is filled with water, the drainage capillary pressure curve can be obtained by reducing the liquid water pressure (or raising the gas pressure). The procedure used in the study involves the following steps (refer also to Fig. 1):

1. With valve 3 closed and valves 1 and 2 open, add water (degassed and deionized) to the straight vertical tube to fill the horizontal graduated tube. Then with valve 2 closed and valves 1 and 3 open, add water to the straight vertical tube until the liquid level reaches the level of the bottom of the sample as close as possible but not above it. It is not necessary to record this amount. The water levels in the chamber and the measurement tube need to be aligned so that no or minimal water is transferred between them when both valves 2 and 3 are opened. When this is achieved, close valve 1 and open valve 2. Record the water level in the horizontal tube and proceed to the next step.
2. Raise the graduated tube slowly in 2 mm increments until the liquid water level in the tube begins to move. Hold the tube steady at this level for at least 10 min to allow water to be displaced from the graduated tube into the chamber or sample. Raise the graduated tube to the next level only when no water movement is observed for at least 5 min. The amount of water displaced is determined from the difference between the original reading and the final reading on the graduated tube.
3. The height of the liquid level above the sample represents the driving force or liquid pressure required to overcome the surface tension at the surface and inside the sample to force this amount of water into the sample. This differential height is used to calculate the liquid pressure. The liquid pressure can also be obtained from the pressure transducer mounted in the chamber of the bottom plate right below the sample. Make correction to the pressure from the transducer for its distance from the bottom surface of the sample if it is not perfectly aligned.
4. The capillary pressure for this sample can be calculated from the following equation, $P_c = P_{nw} - P_w = (P_{water} - P_{air})_{for\ a\ hydrophobic\ medium} = P_{water} - 1$ atm, where P_{water} is the absolute liquid pressure value obtained in step 3. If a gauge pressure sensor is used in step 3, then the pressure reading is also P_c.
5. Repeat steps 2–4 for another height until a desirable saturation level or capillary pressure is obtained.
6. The liquid water saturation level in the sample can be calculated from the following equation, $s = V_{liq}/V_{void} = V_{liq}/(V\varepsilon)$, where V and ε are the total volume and porosity of the sample, respectively. For samples that require higher liquid pressures, instead of steps 2–4 described earlier, a mechanical piston, such as a microsyringe, can also be used. The volume displaced can be measured from the syringe displacement, and the pressure can be obtained with a pressure sensor. The microsyringe technique has been explored by Schwartz's group at the University of Washington.[20,21]

The results obtained from the procedure in steps 1–6 represent the fill-up cycle and not a capillary curve of the sample. However, this curve is necessary in order to establish a known saturation level in the sample. The drainage and imbibition curves are obtained in the subsequent steps and cycles below.

7. To get the first drainage curve, lower the horizontal tube, in increments of 2–5 mm, to reduce the liquid pressure. During this process water is drained from the sample into the graduated tube resulting in an increase in the liquid volume in the tube. Record the change in displaced volume and subtract it from the previous volume to determine the new saturation level in the sample.

8. Repeat step 7 until a desirable drainage capillary pressure range is obtained. If configuration A is used, then the bubble point is reached when gas breaks through the sample causing the liquid phase in the chamber below the sample to separate from the sample. Configuration B will allow measurement of capillary pressures beyond the sample bubble point.

9. When steps 7 and 8 are completed, repeat the procedure in steps 2–6 to obtain the first imbibition capillary pressure curve. If configuration A is used, then this step can be used to determine the liquid water breakthrough point.

10. Multiple imbibition and drainage cycles should be done to ensure that the data are reproducible and to check for hysteresis.

Even with the two ends of the system exposed to water-saturated air, we still had water loss from the system from evaporation. To determine the water loss rate from the system to correct for the volume change, the system was allowed to sit at a slightly positive liquid pressure for 24 h, and the amount of water loss and, consequently, the water loss rate were determined by measuring the volume change in the horizontal tube during this time.

Finally, accurate measurement of the displaced liquid volume in the sample (i.e., liquid saturation level) depends on accurate measurement of the starting point of the volume; that is, the point at which the liquid was assumed to have completely filled the liquid compartment in the end plate below the sample. Any further change in the liquid volume could be assumed to be due to liquid water imbibition into the sample. We have found that the best method to do this was by measuring the inflection point in the liquid pressure vs displaced liquid volume curve. Because the liquid pressure needed for penetration into these carbon materials would exceed the gas pressure for any contact angle of $\gtrsim 50^{\circ}$, there is a significant liquid pressure change at the liquid water penetration point. (We have confirmed that these materials will not spontaneously imbibe water by placing them on top of water in a beaker and finding that no measurable weight gain was observed over a period of 3–24 h.) Prior to this point, no or minimal change in the liquid pressure vs displaced volume was observed as liquid water filled the chamber below the sample (and the hydrophilic layers below the sample when configuration B was used). Once the chamber was completely filled and water came in contact with the sample, the liquid pressure increased sharply until it reached a level high enough to penetrate into the sample.

Figure 3 shows the phenomenon described here. The volume in the horizontal tube at this point was denoted as the starting volume point, and any subsequent changes in the volume were attributed to the volume displaced into the sample. The corresponding liquid pressure was denoted the starting liquid penetration pressure. Note that for the case shown here the starting point could be at the point marked by the arrow or any point between the marked point and the next point. Using smaller elevation steps can reduce this uncertainty. The sample void volume under compression and the starting point constitute the largest sources of errors. We estimated these sources to result in about 10–15% error in the calculation of the liquid water saturation level in the sample.

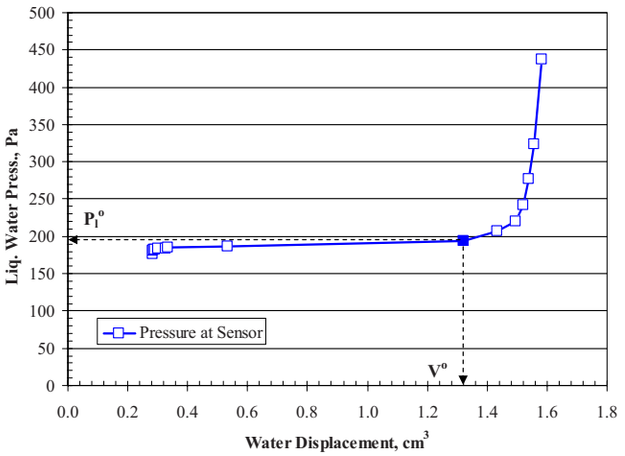

Figure 3. (Color online) Inflection point used to determine the starting imbibition point (darkened).

The procedure above was used to measure the capillary properties of multiple porous carbon gas diffusion materials used in PEMFCs. The capillary pressure curves of two materials widely used in PEMFCs, a highly porous material by SGL Carbon (SIGRACET GDL 10CA) and a less porous, denser material by Toray (TGP-H-060, 10% wet proof), are presented in this paper. Table I shows some of the physical properties of these two materials. The capillary pressure curves of these materials and other materials at different levels of wet proofing, a detailed analysis of the effect of wetproofing levels, and a unifying approach to model the capillary pressure property of these materials will be discussed in a separate paper.

Results and Discussion

Figure 4 shows the capillary pressure curves of a 10% wet proof Toray TGP-H-060 sample obtained after correction for evaporation loss and with the fill-up curve removed. Also included in Fig. 4 is the liquid breakthrough point for this sample and data obtained for the same material by our group in 2007. Note that the measurements are quite reproducible. The liquid breakthrough pressure measured here is within the range reported by Benziger et al. for a similar material.[31] The capillary pressure curves, which are expressed here as $P_c = P_l - P_g$, vs the liquid water saturation level in the sample exhibit the classical S-shape typically observed for hydrophilic materials. The main difference here is that these curves are shifted greatly upward with part of the curves in the hydrophobic region ($P_l > P_g$) and part in the hydrophilic region ($P_g > P_l$). This implies that these porous fibrous carbon materials exhibit both hydro-

Table I. Physical properties of the porous carbon materials used.

Material type	Thickness (μm)	Mean pore size (μm)[a]	Porosity	Permeability (m^2)	Density (g/cm^3)	Surface contact angle (deg)[b]
SGL-10CA	380	~19	0.87	1.89×10^{-12}	0.2505	~135
TGP-H-060	190	~33	0.72	7.75×10^{-12}	0.5105	~130

[a] From the manufacturers.
[b] Measured with deionized water on sample at 22°C.

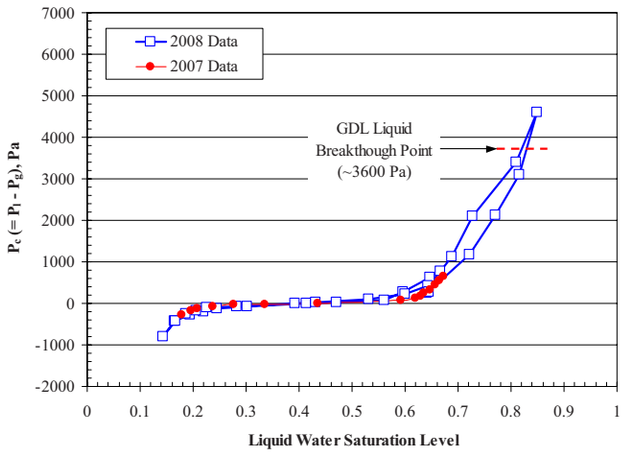

Figure 4. (Color online) Capillary pressure curves after correction for evaporation loss for Toray TGP-H-060 at 22°C.

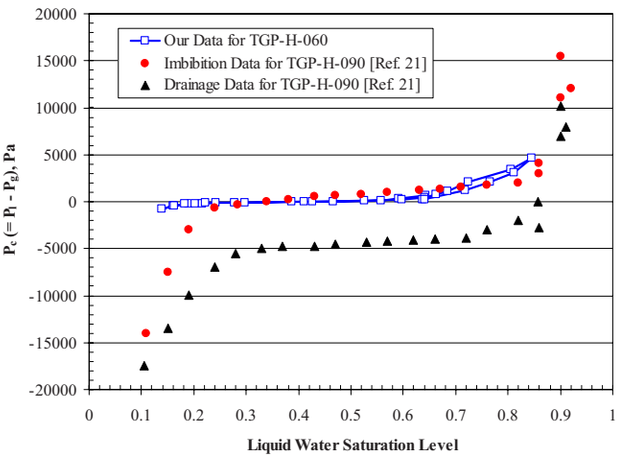

Figure 5. (Color online) Capillary pressure curves for Toray TGP-H-060 and TGP-H-090. Data for TGP-H-090 were extracted from Ref. 21.

philic and hydrophobic properties. This unique property should be taken into consideration in selecting the anode and cathode materials for PEMFCs.

We also noted the following. First, only a fraction of the liquid forced into the sample during the imbibition stage can be removed or drained from the sample by reducing the liquid pressure to that of the gas pressure, that is, the point at which the capillary pressure is equal to zero. Second, the liquid pressure has to be reduced below the gas pressure to continue draining water from the sample. Another way this step can be achieved, as opposed to the process used in this experiment, is by placing the gas diffusion sample in contact with a highly hydrophilic porous material. The fact that this material is hydrophilic means that the liquid in contact with this material is forced to have lower pressure than that of the gas phase and thus helps to drain the liquid out of the gas diffusion sample. This process was used by Gostick et al. at the University of Waterloo[17,18] in their capillary pressure measurements of some selected porous carbon gas diffusion materials. Note that this drainage process only yields the hydrophilic portion of the capillary pressure curve.

Third and final, these samples cannot be completely filled and drained in a fuel cell by these interfacial forces because a condition similar to configuration B does not exist in a fuel cell. Complete liquid drainage can only be achieved by evaporation and complete liquid saturation by blocking the surface of the GDL that is exposed to the gas channel with a hydrophobic layer. Furthermore, the hysteresis observed between the imbibition and drainage curves for these materials was quite small. This is contrary to the results obtained by Schwartz's group at the University of Washington[21] for a similar but slightly thicker Toray material (TGP-H-090) showing significant hysteresis between the drainage and imbibition capillary pressure curves (see Fig. 5).

We are not sure if this difference is due to (*i*) different materials (thickness) used, (*ii*) the effect of the very high and low capillary pressure regions reached in Schwartz's measurements, or (*iii*) the measuring technique used by the University of Washington, in which they pointed out that the system was not quite at pressure equilibrium at every volume increment. Note that our capillary pressure curves for TGP-H-060 agree quite well with the imbibition curve for TGP-H-090 obtained by Schwartz's group. Personally, we think the first attribute is unlikely. The second point could be resolved by cycling between imbibition and drainage at increasingly higher pressure range to see when hysteresis appears, using both this technique and the one used by Schwartz's group. Finally, it is currently not clear to us how hysteresis will affect liquid water transport in the gas diffusion medium and fuel cell performance. This aspect deserves more attention.

Figure 6 shows the capillary pressure curves of a 10% wet-proof carbon paper material (SIGRACET GDL 10CA) from SGL Carbon obtained at 22°C along with the capillary curve of the Toray material shown earlier in Fig. 4. Similar to the Toray material, this porous carbon material also exhibits both hydrophobic and hydrophilic properties. The breakthrough pressure for this material is lower than that of the Toray material and may be attributed to its broader size distribution, especially the sizes of its largest pores.

Within a capillary pressure range the Toray material seems to cover a wider liquid saturation range and reach higher saturation levels than the SGL material. However, the shapes of these capillary pressure curves are similar. The difference in saturation level could be attributed to the differences in their morphological properties. On the basis of our experience with PEMFCs, we could speculate that the Toray material is more suitable for dry feed gas or ambient applications in which it is advantageous to trap liquid water in the GDL to prevent membrane dehydration, and the SGL material to be more suitable for high humidity or saturated feed gas or ambient

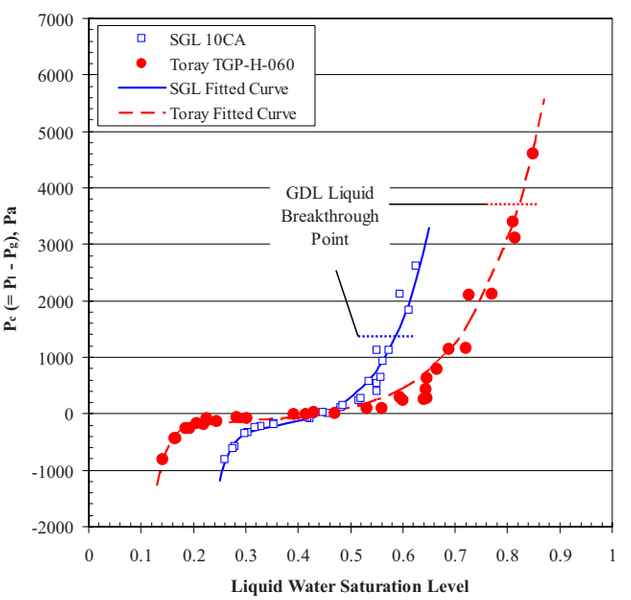

Figure 6. (Color online) Capillary pressure curves of SGL 10CA and Toray TGP-H-060 with fitted curves.

Table II. Fitted values for capillary pressure curves.

Material type	a_1	a_2	b	c[a]	d_1	d_2
SGL-10CA	48.07	11.95	358.3	0.442	0.0781	351.2
Toray TGHP-060	44.02	8.103	191.8	0.496	0.00011	278.3

[a] Midpoint between the maximum and minimum saturation points.

applications. Finally, we are working (*i*) on measuring the capillary pressure at higher temperatures and (*ii*) to identify the relationship between the shape and value of the capillary pressure curve and the morphological and wetting properties of the gas diffusion material.

Also included in Fig. 6 are the fitted curves for these two materials. The equation form used to fit these data is

$$P_c = (P_l - P_g) = d_1 \exp(-a_1[s - c]) - d_2 \exp(a_2[s - c]) + b$$

This correlation was selected because the shape of the capillary pressure curves could be represented by two exponential functions. Furthermore, this form allows the shape of the curves to be easily modified by adjusting the individual parameters to study the effects of the capillary curve shape and magnitude on the liquid water transport characteristics and rate. Similar correlations had been used to fit capillary pressure functions in previous works.[3,4,22,23] In this paper, the correlation was slightly modified to provide a better fit to these experimental data with fewer parameters. Note that this correlation provided a much better fit with fewer parameters than the polynomial forms typically used by other groups.[2,5,8,11,13,14] The parameters a_1 and a_2 were used to scale the shape of the two exponential functions; the parameter c, obtained directly from the experimental data, represents the liquid saturation level at midpoint of the saturation region covered by these curves; the parameters d_1 and d_2 were used to scale the two exponential functions; and the last parameter b was used as an offset to shift the whole capillary pressure curve up or down. The shape and magnitude of the hydrophobic portion can be adjusted by changing the parameters a_1 and d_1, and those of the hydrophilic portion by the parameters a_2 and d_2. The fitted parameters for these two materials are given in Table II. Finally, these correlations could be used in PEMFC models to provide more accurate predictions of the effects of two-phase flow. Recent work has confirmed that the use of actual capillary pressure data in fuel cell models, instead of the correlation by Udell for sand, has led to more accurate predictions of the fuel cell performance over a wide range of operating conditions.[22]

Conclusions

A capillary pressure measurement technique for gas diffusion materials used in PEMFCs was developed. Details on the measurement technique were presented to allow others to reproduce our data and to measure the capillary pressure property of other materials accurately. The capillary pressure property of two commercially available materials, one by SGL Carbon and the other by Toray, was presented. The results show that these gas diffusion materials exhibit both hydrophilic and hydrophobic properties. The shapes of these capillary pressure curves are similar. Their saturation level ranges differ and could be attributed to the differences in their morphological properties. The two-phase transport property of these materials should be considered in selecting materials for the anode and cathode of PEMFCs.

A correlation that allows the shape of these capillary pressure curves to be easily modified by adjusting individual parameters to study the effects of capillary curve shape and magnitude on the liquid water transport characteristics and rate was developed. Fitted values for the capillary pressure curve of two commercial materials were presented. These correlations could be used in fuel cell models to provide more accurate predictions of the fuel cell performance.

Acknowledgments

We thank the SGL Carbon Group for providing some of the materials used in this study. One of the authors, T. V. Nguyen, also acknowledges that the National Science Foundation through the IR/D Program supported the time used to prepare this paper during his assignment at the NSF as a program director.

University of Kansas assisted in meeting the publication costs of this article.

References

1. W. He, J. S. Yi, and T. V. Nguyen, *AIChE J.*, **46**, 2053 (2000).
2. Z. H. Wang, C. Y. Wang, and K. S. Chen, *J. Power Sources*, **94**, 40 (2000).
3. D. Natarajan and T. V. Nguyen, *J. Electrochem. Soc.*, **148**, A1324 (2001).
4. D. Natarajan and T. V. Nguyen, *J. Power Sources*, **115**, 66 (2003).
5. J. H. Nam and M. Kaviany, *Int. J. Heat Mass Transfer*, **46**, 4595 (2003).
6. T. Berning and N. Djilali, *J. Electrochem. Soc.*, **150**, A1589 (2003).
7. A. Z. Weber and J. Newman, *Chem. Rev. (Washington, D.C.)*, **104**, 4679 (2004).
8. C. Y. Wang, *Chem. Rev. (Washington, D.C.)*, **104**, 4727 (2004).
9. G. Lin, W. He, and T. V. Nguyen, *J. Electrochem. Soc.*, **151**, A1999 (2004); G. Lin, W. He, and T. V. Nguyen, *J. Electrochem. Soc.*, **153**, L12 (2006).
10. R. Jain and T. Nguyen, *ECS Trans.*, **1**(6), 463 (2005).
11. U. Pasaogullari, C. Y. Wang, and K. S. Chen, *J. Electrochem. Soc.*, **152**, A1574 (2005).
12. G. Lin and T. V. Nguyen, *J. Electrochem. Soc.*, **153**, A372 (2006).
13. Y. Wang and C. Y. Wang, *J. Electrochem. Soc.*, **153**, A1193 (2006).
14. H. Ju, G. Luo, and C. Y. Wang, *J. Electrochem. Soc.*, **154**, B218 (2007).
15. A. Z. Weber, R. M. Darling, and J. Newman, *J. Electrochem. Soc.*, **151**, A1715 (2004).
16. H. Ohn, T. Nguyen, D. Hussey, D. Jacobson, and M. Arif, *ECS Trans.*, **1**(6), 481 (2005).
17. J. T. Gostick, M. W. Fowler, M. D. Pritzker, M. A. Ioannidis, and L. M. Behra, *J. Power Sources*, **162**, 228 (2006).
18. J. T. Gostick, M. A. Ioannidis, M. W. Fowler, and M. D. Pritzker, *J. Power Sources*, **173**, 277 (2007).
19. T. V. Nguyen, G. Lin, H. Ohn, X. Wang, D. S. Hussey, D. L. Jacobson, and M. Arif, *ECS Trans.*, **3**(1), 415 (2006).
20. J. D. Fairweather, P. Cheung, D. T. Schwartz, and J. St-Pierre, *ECS Trans.*, **3**(1), 981 (2006).
21. J. D. Fairweather, P. Cheung, J. St-Pierre, and D. T. Schwartz, *Electrochem. Commun.*, **9**, 2340 (2007).
22. Q. Ye and T. Van Nguyen, *J. Electrochem. Soc.*, **154**, B1242 (2007).
23. X. Wang and T. V. Nguyen, *ECS Trans.*, **11**(1), 693 (2007).
24. E. C. Kumbur, K. V. Sharp, and M. M. Mench, *J. Electrochem. Soc.*, **154**, B1295 (2007).
25. E. C. Kumbur, K. V. Sharp, and M. M. Mench, *J. Electrochem. Soc.*, **154**, B1305 (2007).
26. E. C. Kumbur, K. V. Sharp, and M. M. Mench, *J. Electrochem. Soc.*, **154**, B1315 (2007).
27. K. S. Udell, *Int. J. Heat Mass Transfer*, **28**, 485 (1985).
28. N. R. Morrow and N. Mungan, Report no. RR-7, Petroleum Recovery Research Institute, Calgary, Canada (1971).
29. N. R. Morrow, *J. Can. Pet. Technol.*, **15**, 49 (1976).
30. W. G. Anderson, *JPT, J. Pet. Technol.*, **39**, 1283 (1987).
31. J. Benziger, J. Nehlsen, D. Blackwell, T. Brennan, and J. Itescu, *J. Membr. Sci.*, **261**, 98 (2005).